

Phase-Averaged Mixing and Combustion Characteristics of Multiple Jets Perturbed by Cyclic Oscillation

Masaaki MIZUNO, Kazuya TATSUMI, Shinya OKANO and Kazuyoshi NAKABE

Department of Mechanical Engineering and Science, Kyoto University, Kyoto 606-8501, Japan

Abstract

In the present study, flow and flame characteristics of a jet array, which consists of three jets arranged in a row, were evaluated. Methane and air were supplied from the center and two side jets, respectively. The effects of periodically pulsating the flow rate of the side air jets were examined under very small Strouhal number based on the time-mean jet velocity. Schlieren photographs were taken by a high-speed digital video camera in the cases when combustion was accompanied. Flow velocity distributions in non-combustion cases were obtained using laser-Doppler velocimetry. Small effects of the pulsating flow were observed in non-combustion state under such small Strouhal number discussed in the present study. However, larger effect on the flow patterns was observed when combustion reaction was accompanied, particularly changing the location of the flow transition from laminar to turbulent.

Key words

Multiple jet array, Jet flame, Pulsating flow, Laser-Doppler velocimetry, Schlieren photographs

1. Introduction

Mixing between multiple jets is fundamental and important phenomena in fluid dynamics. It appears in various industrial applications and is an essential factor that significantly affects the device performances. For example, poor mixing between jets of fuels and oxidation in a combustor incurs a deterioration of the combustion efficiency and emission of toxic substances such as unburned hydrocarbons, soot and carbon monoxide. Particularly, under low Reynolds number conditions, the flow becomes laminar, and a marked deterioration of the mixing performance takes place among the jets due to the lack of turbulence mixing. These low Reynolds number jet flows are found in small size applications (e.g. micro gas turbine, chemical mixing devices and μ -TAS) owing to the small characteristic length scale of the jet nozzles.

To tackle this problem, several techniques have been suggested and studied in the past decades. Choi et al. [1] proposed a novel miniature-size can-type combustor consisting of millimeter-scale confined multiple jets. In this combustor, a baffle plate consisting of several nozzle holes was introduced, and the fuel and air were respectively supplied from the baffle plate through the nozzles to the combustion chamber. The mixing performance was markedly improved in this system mainly due to the interaction between each jet [2]. In order to investigate the effects of such jet interactions upon the jet fluid mixing, the velocity distributions in triple jets arrayed simply in line were measured by Nakabe et al. [3]. In this case, the interaction between the jets moved the laminar-turbulent transition region upstream compared

with a single jet case. They also reported that an earlier transition of the jet flow from laminar to turbulent and also a jet bifurcation were observed by applying a minimal cyclic perturbation to the flow using acoustic waves. Recently, Tatsumi et al. [4, 5] studied the effects of pulsating the mass flow rate of the jets on the unsteady characteristics of the multi-jets under the conditions of large amplitudes and very low Strouhal number based on the time-mean jet velocity. Although the effects were not so large compared with those produced by the acoustic excitation [3], the large temporal fluctuation of jet flow affected the time-mean mixing performance of the jets, particularly in the area adjacent to the nozzle exit.

The above characteristics were discussed under the conditions without combustion reaction. The effects of the interaction between the jets and flow-perturbation on the characteristics of the multi-jets can be more significant in combustion state due to the existence of the physical properties variation in the flow, particularly at the flame surface. In the present study, therefore, experiments were conducted to evaluate the aforementioned effects on a triple-jets arrayed in line. Visualization of the combustion field applying the Schlieren method to the multi-jets was conducted. Furthermore, flow velocity measurements using laser Doppler velocimetry were carried out to evaluate the pulsating flow effects on the air-jet mixing characteristics in non-combustion state, to discriminate the interaction effect between the pulsating jets and jet flame from the basic flow characteristics of the multi-jet.

2. Experimental apparatus and conditions

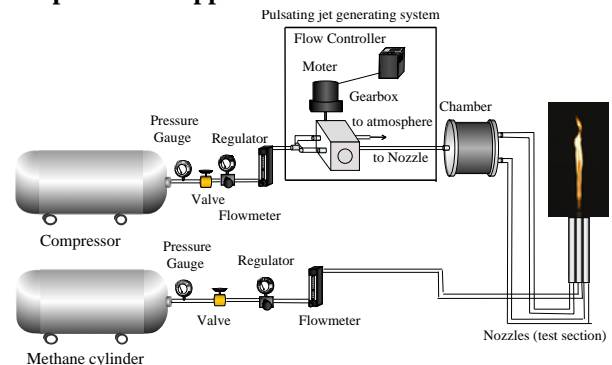


Fig. 1: Experimental apparatus.

Figure 1 shows the experimental apparatus of the present study. The triple jet nozzles aligned in the apparatus was employed as the measuring object, which was the same as the above mentioned experiments done by Tatsumi et al [4, 5]. Figure 2 illustrates the magnified view of the nozzle arrangement. Three jets nozzles were aligned in a row, and the jets were blown into the stationary atmosphere, which was an open, wide and calm space. The nozzles were situated in parallel with the same inner diameter of d

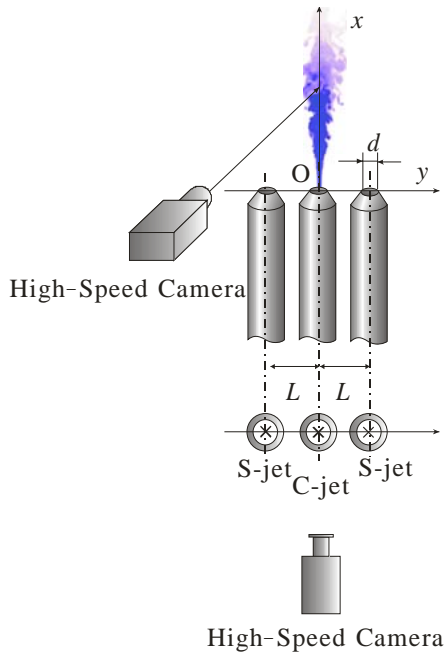


Fig. 2: Nozzle arrangement.

= 4mm, constituting a triple jet array. The nozzle tip was sharpened and tapered by 45 degrees. As convenient for further discussion, hereafter, the center jet will be referred to as C-jet and the two other side jets will be referred to as S-jets. The separation distance between the center of C-jet and S-jets, L , was fixed at 6.0mm.

Air was supplied from a compressor to the S-jets. To C-jet, methane gas and air were respectively supplied under each condition of non-combustion and combustion states. The flow rates of these gases were controlled by a flow meter located at the upstream of the nozzles.

The pulsating jet flow was generated by a pulsating flow generating unit, which was installed upstream of the jets as indicated by the black frame in Fig. 1. Figure 3 shows the schematic view of this unit. The unit was composed of a cylinder and chassis. Through-holes were made at the side walls of the cylinder and chassis, and their locations corresponded to each other. The cylinder was connected to a DC electric motor (Oriental Motor, MSD425-401D), and was rotated under constant angular speed. The flow rate was, thus, changed periodically depending on the crossover area between the holes of the cylinder and chassis. Note that a bypass hole was drilled aside the main flow passage so that in the phase when the area of the main flow passage was decreased, the area of the bypass hole was increased and large amount of flow was discharged to the atmosphere. This prevented an increase of the upstream pressure which caused an undesired pulse in the velocity profiles of pulsating flow. The frequency of jet perturbation was controlled by the rotation speed of the cylinder.

As shown in Fig. 3, a laser motion detection sensor (KEYENCE, LV-51M) was employed on the pulsating flow generating unit. A needle-shape marker was attached to the rotating cylinder that intersected the aforementioned

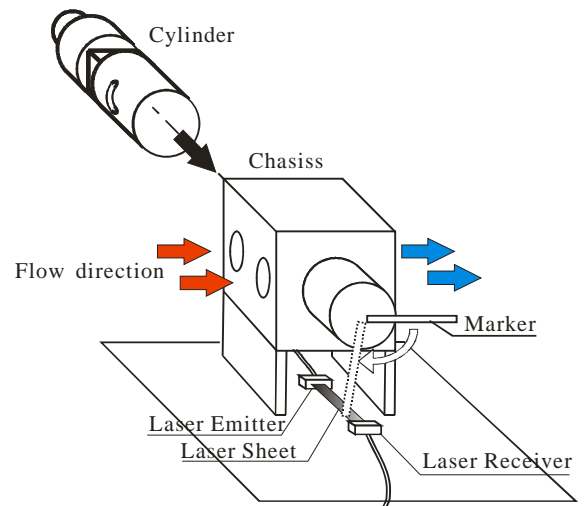


Fig. 3: Schematic view of pulsating flow generating unit.

laser sensor at each period of the cylinder rotation. The trigger signal from the sensor was sent to the high-speed digital camera used in the Schlieren method and to the mechanical shutter placed at the exit of the laser unit used in the laser Doppler velocimetry (LDV) measurements. In each measurement, this trigger signal was used to start the data recording, and to synchronize the data signals with the phase of the pulsating flow.

Figure 4 shows the schematic view of the system of the Schlieren method employed in the combustion experiments. An Ar-ion laser (Spectra Physics, model2017L-AR) was employed as the light source. The laser beam was first lead through a converging lens and pinhole, by which a point light source was produced. The light was then changed to a parallel light by a concave mirror, as shown in Fig. 3 described as CM1. The diameter and focal length of this mirror were 300mm and 3,000mm, respectively. The parallel light passing the test section was then converged by another concave mirror, CM2, and was guided to the high speed camera. A knife edge, KE, was placed at the focal point located at the camera upstream to intensify the contrast produced by the gas density difference in the image. KE was made of a glass plate, onto which a 2mm size square pattern was printed as shown in Fig. 4 (b). The Schlieren photographs were taken by a high speed camera (Vision Research, Phantom V7.3). The exposure time of the camera was 2 μ s and the frame rate was 1,000 frames per second. The resolution of the captured images was approximately 1.3mm per pixel.

In non-combustion experiments, the flow velocity was measured by the LDV system. In this system, two pairs of laser beams (wave length = 488.0nm and 514.5nm) emitted from the aforementioned Ar-ion laser were guided to the test section. The Doppler burst signals of the scattering light from the tracer particles obtained by a receiver probe were recorded and analyzed by a signal processor (DANTEC, BSA F50), which was linked to and controlled by a personal computer. To mix tracer particles in the working fluids, a particle generator (TSI,

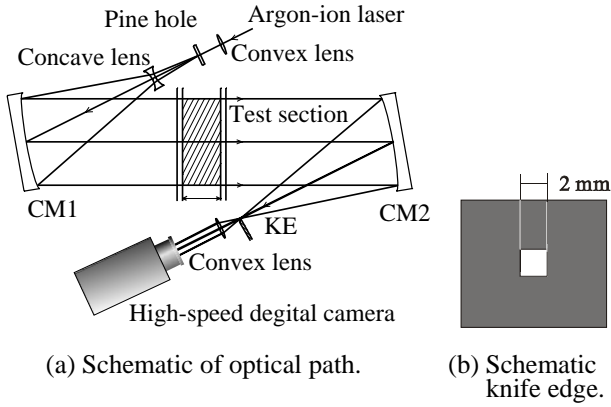


Fig. 4: Apparatus of Schlieren method.

model9306) was installed downstream of flow meters. The particles used in the present study were oil mist of Di-Ethyl-Hexy-Sebacate ($1.0\mu\text{m}$ in nominal diameter). As mentioned before, the start of the LDV measurement was synchronized with the pulsating jet by a mechanical shutter (Suruga Seiki, F116), to which the trigger signal was sent from the laser sensor.

Table 1 shows the experimental conditions discussed in the present study. The characters “St” and “P” used in Table 1 indicate the flow conditions of the jets: steady and pulsating states. The titles “air” and “flame” indicate respectively the jets under non-combustion and combustion conditions. Largely grouped, three cases were examined in the present study. The first one is a single jet blown out from the C-jet nozzle under steady state condition (the case of 1S). The second one is triple jets discharged from the nozzles of the C-jet and S-jets under steady state conditions (the case of 3S). The last one is triple jets (the case of 3P), in which a steady jet was provided from the nozzles of C-jet and pulsating jets were supplied from S-jets.

The Reynolds number of the steady jet was fixed at a constant value, $Re = 1.5 \times 10^3$. Re was calculated on the basis of the nozzle diameter d and time-mean streamwise velocity at the center of the C-jet nozzle outlet ($x/d = 0.25$ and $y/d = 0$). In the pulsating jet case, the mean Reynolds number was 1.5×10^3 . In this case, the characteristic velocity was the half value of the time-mean streamwise velocity at the center of the S-jet nozzle outlet ($x/d = 0.25$ and $y/d = \pm 1.5$). The frequency of the pulsating jet, f , was 1Hz. The kinetic viscosity was calculated under the condition of the atmosphere temperature.

Table 1: Experimental conditions.

Case	1S-F	3S-F	3P-F	1S-A	3S-A	3P-A
C-jet	St-flame	St-flame	St-flame	St-air	St-air	St-air
S-jets	—	St-air	P-air	—	St-air	P-air

3. Results and discussion

3.1 Schlieren photographing in combustion experiments

Figure 5 shows the Schlieren photographs of the flames obtained in the cases of (a) single and (b) triple jet arrays

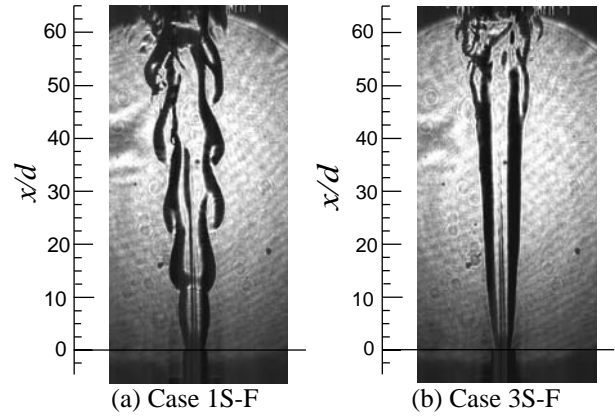


Fig. 5: Schlieren photographs in steady jet flame cases.

under steady state flow conditions (the cases of 1S-F and 3S-F). In the case of 1S-F, generation of large scale periodical fluctuations are observed at the boundary surface of the fuel and surrounding air. This is believed to be attributed to velocity increase of the jet fluid relative to the ambient fluid due to the decrease of the fluid density produced by the local temperature increase of the flame. On the other hand, in the case of 3S-F, such fluctuations are not observed. A smooth surface is formed along the streamwise direction from the exit of the nozzles to the location of $x/d \sim 40$. This implies that in the multi-jet case, the suppression of the flame surface fluctuating is attained by the assist of air-supply jets along the sides of a fuel jet.

In Fig. 6, the time-sequential Schlieren images obtained in the case of 3P-F are shown. T described in the figure presents the time period of one cycle of the pulsating flow. T is estimated using the distribution of auto-correlation function, $C(\tau)$, that is defined as the following equation using the instantaneous streamwise velocity, $U(t)$.

$$C(\tau) = \frac{1}{t_2 - t_1} \int_{t_1}^{t_2} U(t)U(t + \tau) dt \quad (1)$$

In Eq. (1), $t_2 - t_1$ indicates the time span of the LDV measurement.

Figure 7 shows the distributions of the time history of the phase-averaged streamwise velocity \tilde{U} monitored at the center of the nozzle exit ($x/d = 0.25$, $y/d = 0$) of C-jet and S-jet, respectively. Both values are obtained in the case of 3P-A. The values in the figure are normalized by U_0 that represents the time-mean streamwise velocity obtained at the nozzle exit center of the C-jet under the steady state case of 3S-A.

Although not shown here, according to the streamwise turbulence intensity, $\sqrt{u'^2}$, obtained at the nozzle exit, the jet was considered to be laminar during the period of $0.4 \leq t/T \leq 0.9$. On the contrary, during the periods of $0 \leq t/T \leq 0.4$ and $0.9 \leq t/T \leq 1.0$, $\sqrt{u'^2}$ was markedly increased, and, therefore, a turbulent jet was expected to be discharged from the nozzle. The relation among \tilde{U} , $u'(t)$ and turbulence intensity, $\sqrt{u'^2}$, and the definition of $\sqrt{u'^2}$ used in the present study are described in Eqs. (2) and (3).

$$U(t) = \bar{U} + U'(t) = \tilde{U} + u'(t) \quad (2)$$

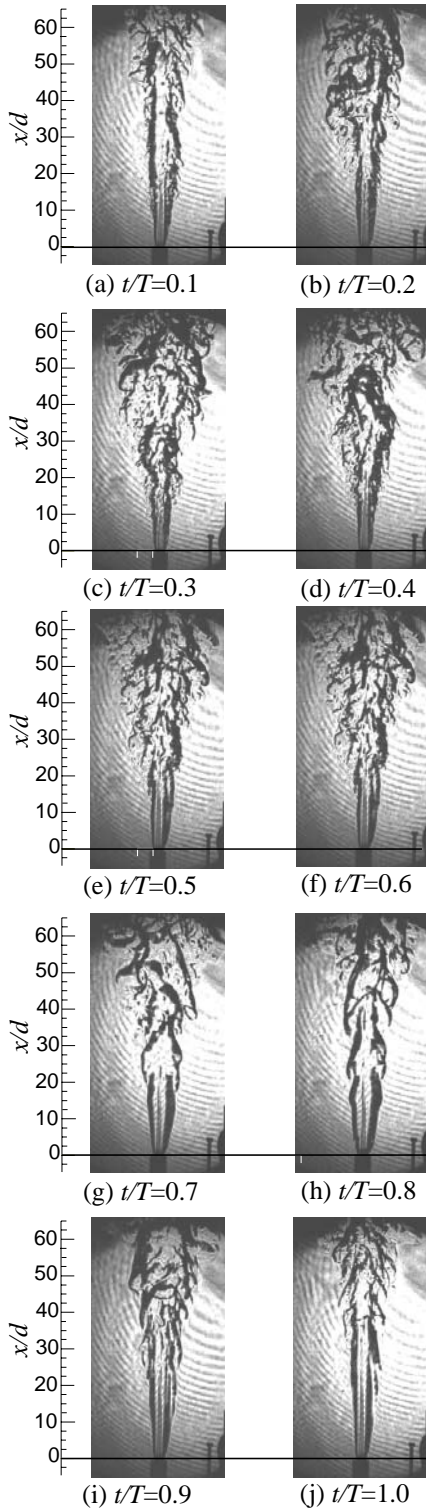


Fig. 6: Time-sequential Schlieren images of jet flame with pulsating air-jets (the case of 3P-F).

$$\sqrt{u'^2} = \sqrt{\frac{1}{t_2 - t_1} \int_{t_1}^{t_2} (U(t) - \tilde{U}(t))^2 dt} \quad (3)$$

At $t/T = 0.1 \sim 0.4$, which is the period that \tilde{U} is relatively large and a turbulent jets is formed from the nozzle exit of S-jets, ripples appear at the boundary between fuel and air from the area of $x/d = 10 \sim 20$ in spite

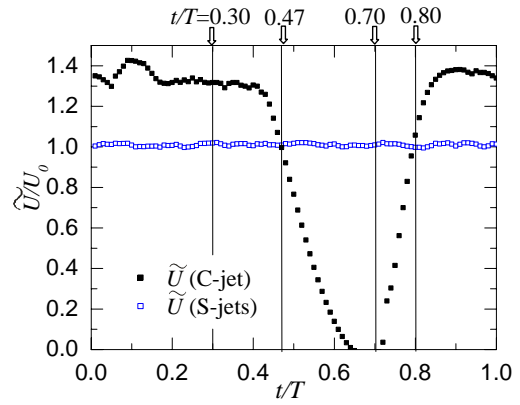


Fig. 7: \tilde{U} of C-jet and S-jets measured at the nozzle center and $x/d = 0.25$ in the case of 3P-A.

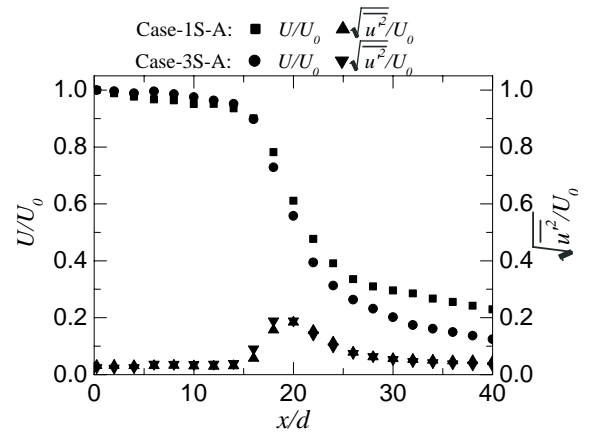
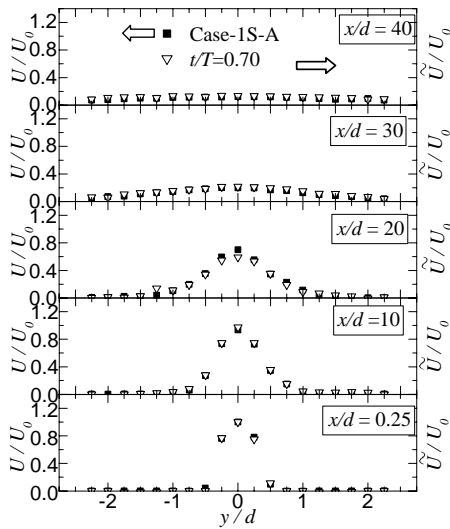


Fig. 8: Streamwise distributions of \tilde{U} / U_0 and $\sqrt{u'^2} / U_0$ at center of C-jet and S-jets.

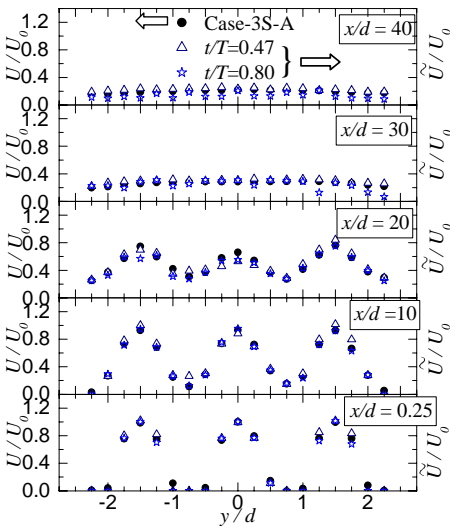
of unclearly visualized images in Fig. 6 (a) ~ (d). At the location further downstream of these jets, generation of various length-scale vortices becomes recognizable, which indicates that the jet flame is turbulent. During the period when the S-jets are accelerating, i.e. at $t/T = 0.7$ and 0.8 of Fig. 6 (g) and (h), large scale fluctuations are observed at the boundary surface of the flame in the area of $0 \leq x/d \leq 30$. Production of such periodical fluctuation at the flame surface is a common characteristic similar to that obtained in the case of 1S-F shown in Fig. 5 (a). During the period when the S-jets are decelerating, i.e. at (e) $t/T = 0.5$ and (f) $t/T = 0.6$ of Fig. 6, the flame images appear a bit different, compared to the ones in the accelerating period. Some traces of typical turbulent flame's feature remains in this period, particularly in the region beyond half-way downstream of the flame. More detail investigation should be necessary in the near future. At $t/T = 0.9, 1.0$ shown in Fig. 6 (i) and (j), the flame shows a common behavior that observed in the case of 3S-F shown in Fig. 5 (b). Namely, a smooth flame surface is developed at the nozzle downstream to the region of $0 \leq x/d \leq 30$.

3.2 Comparison of the multi-jet flow characteristics in combustion state with in non-combustion state

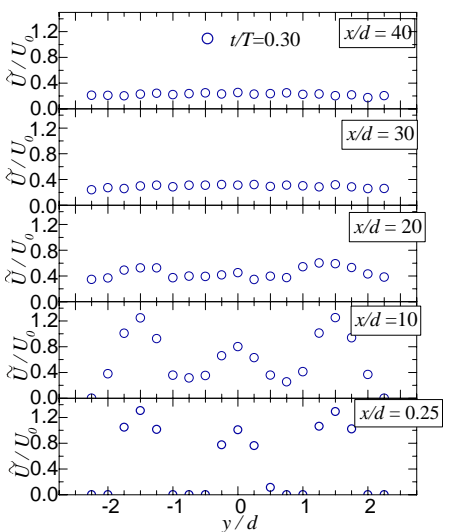
In this section, comparisons of the flow characteristics of the multi-jets obtained in the cases under the conditions of combustion and non-combustion states are conducted to



(a) U/U_0 in the case of 1S-A and \tilde{U}/U_0 in the case of 3S-P at $t/T = 0.70$.



(b) U/U_0 in the case of 3S-A and \tilde{U}/U_0 in the case of 3S-P at $t/T = 0.47, 0.80$.



(c) \tilde{U}/U_0 in the case of 3S-P at $t/T = 0.30$.

Fig. 9: Spanwise distribution of the streamwise velocity at each cross-section.

evaluate the interaction effects of the flame and pulsating jet flows.

Figure 8 shows the streamwise distributions of time-mean streamwise velocity, \bar{U}/U_0 , and turbulence intensity, $\sqrt{u'^2}/U_0$, obtained along the centerline of C-jet ($y = 0$) in the cases of 1S-A and 3S-A. The solid square and triangle symbols (\blacksquare and \blacktriangle) indicate respectively \bar{U}/U_0 and $\sqrt{u'^2}/U_0$ obtained in the case of 1S-A. The solid circle and inverted triangles (\bullet and \blacktriangledown) represent respectively \bar{U}/U_0 and $\sqrt{u'^2}/U_0$ in the case of 3S-A. Figure 9 shows the comparison of the spanwise distributions of the streamwise velocity at five streamwise locations, i.e., $x/d = 0.25, 10, 20, 30$ and 40 . The time-mean streamwise velocity, \bar{U}/U_0 , of the cases of 1S-A and 3S-A are shown in Fig. 9 (a) and (b), respectively. The phase-averaged velocity, \tilde{U}/U_0 , obtained in the case of 3P-A at the time periods of $t/T = 0.70, 0.47, 0.80$ and 0.30 are plotted using open symbols, ∇, \triangle, \star and \circ , in Fig. 9 (a), (b) and (c).

In Fig. 8, \bar{U}/U_0 decreases markedly in the streamwise locations of $15 \leq x/d \leq 25$ in the cases of 1S-A and 3S-A. $\sqrt{u'^2}/U_0$ increases approximately at the same location and takes a maximum value at $x/d \approx 20$. In Fig. 9 (b), the maximum peaks of \bar{U}/U_0 distribution located downstream of each jet center decreases in the area of $10 \leq x/d \leq 20$ in the case of 3S-A, and a relatively flat pattern in the spanwise direction is obtained further downstream. Transition of the jet from laminar to turbulent is, therefore, expected in this region, and a larger diffusion effects is obtained in the spanwise direction in the case of 3S-A. In the results of triple jets in combustion state (the case of 3S-F), a smooth flame surface was produced in the region of $x/d \leq 40$ as represented in Fig. 5 (b), due to the effects of the neighboring air-jets. Comparing the locations of the area where the transition of the jet from laminar to turbulent, one can find that it is located downstream in the case of 3S-F compared with the case of 3S-A. The main reason for this is believed to be due to the variation of the properties of the fluid owing to the temperature increase of the flame. By this, the kinetic viscosity increased and the reduction of the local Reynolds number was obtained that induced a laminarization of the flow. Therefore, the interaction effects, and namely mixing, between the neighboring jets deteriorates in combustion state.

The effects of perturbation in non-combustion states will be considered. Comparing the streamwise velocities shown in Fig. 9 (a), the distributions of \bar{U}/U_0 of the case of 1S-A are nearly equivalent to those of \tilde{U}/U_0 obtained in the case of 3P-A at $t/T = 0.70$. Comparing the streamwise velocities shown in Fig. 9 (b), the distributions of \bar{U}/U_0 obtained in the case of 3P-A at $t/T = 0.47$ and 0.80 are nearly equivalent to those obtained in the case of 3S-A. In the former case, the flow rate of S-jets is approximately zero as shown in Fig. 7, i.e., only C-jet is discharged. In the latter case, the instantaneous Reynolds numbers of S-jets are identical with those of the case of 3S-A that can be estimated from Fig. 7. The instantaneous flow characteristics of the triple jets are, therefore, roughly equivalent between the cases under steady and

pulsating conditions if the Reynolds numbers are the same. These results suggest that the effects of perturbation on the flow characteristics in the triple jet array under non-combustion conditions are small during the time phase of $0.4 \leq t/T \leq 0.9$ when the Strouhal number is small with the present perturbation patterns. These results are different from those obtained by Tatsumi [4, 5], one possible reason of which will be due to the difference of pulsating pattern. More detail investigation will be needed.

In combustion states, first, Fig. 6 (g) (the case of 3P-F at $t/T = 0.7$) and Fig. 5 (a) (the case of 1S-F) are compared. In both cases, the instantaneous flow rate of S-jets is nearly zero. As mentioned in the previous section, large scale fluctuation is found at the fuel-air jets boundary in both cases. However, while the large scale vortices were periodically observed from the nozzle exit to downstream in Fig. 5 (a) (the case of 1S-F), such large scale vortices are only partially observed in Fig. 6 (g) and the conditions of flame were different in each region.

Next, the image of Fig. 6 (e) and (h) (the image of the case of 3S-F at $t/T = 0.5$ and 0.8) are compared with Fig. 5 (b) (the case of 3S-F). Although the instantaneous flow rates of S-jets are approximately identical as is indicated in Fig. 8, a difference in the flow characteristics between these three photographs is observed. The transition regions of the flow from laminar to turbulent shown in Fig. 6 (e) and (h) are located further upstream than that the region shown in Fig. 5 (b). This result indicates that during the period even when the instantaneous flow rate is equivalent in the cases of 3P-F and 3S-F, a different flow are obtained in the multi-jets when combustion is accompanied. This differs to the results obtained in the non-combustion case previously discussed. Therefore, the effects on flow characteristics of the perturbation produced by the side air-jets are believed to be more significant in combustion states.

4. Conclusions

The flow characteristics of a triple jet array accompanied by a pulsating neighboring jets in combustion and non-combustion state have been experimentally investigated. The flow Reynolds number was fixed at 1.5×10^3 and pulsating frequency was $f = 1\text{Hz}$ in the present study. The major findings are summarized as follows:

- 1) In the steady triple jets cases, the region where the transition of jet flow from laminar to turbulent occurs was located further downstream under the condition with combustions, compared with the case of non-combustion air jet array. This is due to the increase of the local fluid temperature gained by the combustion reaction.
- 2) The phase-averaged streamwise velocity distributions of the jet array with pulsating jet in non-combustion state were nearly equivalent to those obtained in the steady jet case during the period when the instantaneous flow rate of the pulsating jet was identical with that of the steady jet cases. Therefore, the effects of flow pulsation were considered to be small in non-combustion states under very small Strouhal number and the present pulsation pattern.
- 3) The instantaneous flame characteristics of the jet flame array with pulsating jet were different from those obtained

in the steady jet flame array, even under the conditions of the instantaneous flow rate of the pulsating jet to be the same as that in the steady cases. The effects of the pulsating flow were considered to be larger when a combustion reaction is accompanied, compared with non-combustion jet array. Acceleration and deceleration effects of the neighboring air jet pulsation might have additional interesting influences on the combustion characteristics of the central fuel jet.

Nomenclature

d	nozzle diameter, m
f	perturbation frequency, Hz
L	separation distance between nozzles, m
Re	jet Reynolds number, $U_m d / \nu$
U	time-mean streamwise velocity of jet, m/s
u'	streamwise velocity fluctuation, m/s
V	time-mean lateral velocity, m/s
v'	lateral velocity fluctuation, m/s
x	streamwise distance, m
y	lateral distance, m
t	instantaneous time, s
T	time-period of jet perturbation, s

Subscripts

0 time-mean reference value at the jet center

Superscripts

~ phase-averaged value

Acknowledgements

This research was partially supported through Grand-in-aid for Scientific Research (B) by Ministry of Education, Culture, Sports, Science and Technology. The authors express their gratitude here.

References

- [1] Choi, H.-S., Katsumoto, Y., Nakabe, K. and Suzuki, K., An Experimental Investigation of Mixing and Combustion Characteristics on the Can-Type Micro Combustor with a Multi-Jet Baffle Plate, *Fluid Mechanics and Its Applications – Turbulent, Mixing and Combustion* -, 70 (2002), 367-375, Kluwer Academic Publisher.
- [2] Woodfield, P.L., Nakabe, K. and Suzuki, K., Numerical Study for Enhancement of Laminar Flow Mixing Using Multiple Confined Jets in a Micro-Can Combustor, *Int. Journal of Heat and Mass Transfer*, 46(2003), pp. 2655-2663.
- [3] Nakabe, K., Kitaoka, Y., H.S. Choi and Suzuki, K., Experimental Study on Flow Characteristics of a Micro Jet Deformed by the Interaction with the Neighboring Jets, *Proc. of the 6th ASME-JSME Thermal Eng. Conf.*, TED-AI03-637 (2003).
- [4] Tatsumi, K., Shinohara, E., Mizuno, M., Nakabe, K., phase-averaged Mixing Characteristics of Multi-Jets Modified by Cyclic Perturbation, *JSME Int. J., Ser. B*, (2006), 49-4, 959-965.
- [5] Tatsumi, K., Shinohara, E., Mizuno, M. and Nakabe, K., Phase-Averaged Mixing Characteristics of Multi-Jets Modified by Cyclic Perturbation, *Japanese Society for Experimental Mechanics*, (2007), 7, 6-11.